International Journal of Science Engineering and Advance Technology

A Voltage Oriented Control Method for PV - Grid Interfaced Inverter by Using Advanced MPPT Algorithm

HIMA BINDU S
P.G. scholar, Dept of EEE
Trr College of Engineering & Technology,
Hyderabad, Telangana, India

BHARGAV RAM T
Associate professor, Dept of EEE
Trr College of Engineering & Technology,
Hyderabad, Telangana, India

*Abstract:-***The output power of PV module varies with module temperature, solar irradiation and loads. And in order to quickly and accurately track the sun, it is necessary to track the maximum power point (MPP) all the time. An improved maximum power point tracking (MPPT) with better performance based on voltage-oriented control (VOC) is proposed to solve a fast changing irradiation problem. In VOC, a cascaded control structure with an outer dc link voltage control loop and an inner current control loop is used. The MPPT controller is applied to the reference of the outer loop control dc voltage photovoltaic (PV). In this project, the main component of the single-stage grid connected PV system is the three-phase voltage source inverter (VSI). The voltage-oriented control (VOC) method used for VSI employs an outer dc link voltage control loop and an inner current control loop to achieve fast dynamic response. The performance of the power flow depends largely on the quality of the applied current control strategy. In this project, the current control has been implemented in a rotating synchronous reference frame d, q because the controller can eliminate a steady-state error and has fast transient response by decoupling control. The robust tracking capability under rapidly increasing and decreasing irradiance is verified in simulations. Simulation results on a large-scale grid-connected PV system show the effectiveness of the proposed control scheme in terms of delivering maximum power into the grid under variable conditions.**

I. INTRODUCTION

Due to global concern on climate change and sustainable electrical power supply, renewable energy is increasingly getting popular in the developed countries. Among different sources of renewable energy, PV system is a promising energy source in the recent years as PV installations are increasing due to their environment friendly operation. Grid-connected PV system has gained popularity due to the feed-in-tariff and the reduction of battery cost. However, the intermittent PV generation varies with the change in atmospheric conditions.

The voltage-power characteristic of a photovoltaic (PV) array is nonlinear and time varying because of the changes caused by the atmospheric conditions. The task of a maximum power point (MPP) tracking (MPPT) in a PV power system is to continuously tune the system so that it draws maximum power from the PV array.

Maximum Power Point Tracking, frequently referred to as MPPT, is an electronic system that operates the Photovoltaic (PV) modules in a manner that allows the modules to produce all the power they are capable of. MPPT is not a mechanical tracking system that “physically moves” the modules to make them point more directly at the sun. MPPT is a fully electronic system that varies the electrical operating point of the modules so that the modules are able to deliver maximum available power. Additional power harvested from the modules is then made available as increased battery charge current.

In recent years, the grid connected PV systems have become more popular because they do not need battery backups to ensure MPPT. The two typical configurations of a grid-connected PV system are single or two stages. In two stages, the first is used to boost the PV array voltage and track the maximum power; the second allows the conversion of this power into high-quality ac voltage.

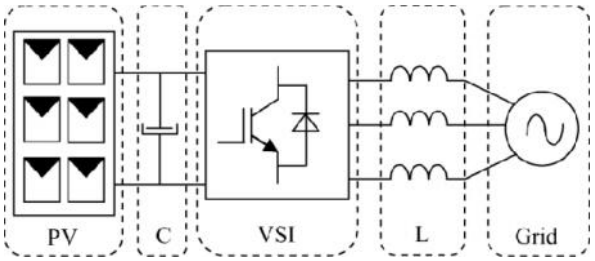

Figure 1: Block diagram of a single-stage grid-connected PV system.

The presence of several power stages undermines the overall efficiency, reliability, and compactness of the system besides increasing the cost. The single stage has numerous advantages, such as simple topology, high efficiency, etc. Nevertheless, the control strategy has to be designed in order to extract the maximum available power and to properly transfer it from the PV array to the grid simultaneously. In this case, an important consideration in the controller design is needed.

In this paper, the main component of the single-stage grid connected PV system is the three-phase voltage source inverter (VSI). Typically, simple inductors *L* are used as a filter interfacing inverter and mains, as shown in Fig. 1. *LCL* filter provides advantages in costs and dynamics since smaller inductors can be used. However, in a grid-connected system, an *LCL* filter may cause resonance, which is a disaster for the system's stability [4]. Hence, control systems involving *LCL* filters are inevitably more complicated. The voltage-oriented control (VOC) method used for VSI employs an outer dc link voltage control loop and an inner current control loop to achieve fast dynamic response. The performance of the power flow depends largely on the quality of the applied current control strategy. In this paper, the current control has been implemented in a rotating synchronous reference frame *d*, *q* because the controller can eliminate a steady-state error and has fast transient response by decoupling control.

A number of techniques are available in the literature for designing the MPPT. Perturb and observe (PO), and incremental conductance method are commonly used techniques in the area of photovoltaic systems. Among the MPPT techniques, the perturbation and observation (P&O) method is the most popular because of the simplicity of its control structure. Yet, in the presence of rapidly changing atmospheric conditions, the P&O MPPT algorithm can be confused due to the fact that it is not able to distinguish the variations of the output power caused by the tracker perturbation from those caused by the irradiance variation. Recently, improved P&O MPPT algorithms for rapidly changing environmental conditions have been proposed by Sera *et al*. The drawback of this P&O method is the necessity of performing an additional measurement of power in the middle of the MPPT sampling period to separate the effects of the irradiation change from the effect of the tracker perturbation.

In this paper, in order to generate the correct MPP reference voltage under rapidly changing irradiation, a robust MPPT controller has been proposed. In this algorithm, the *d*-axis grid current component reflecting the power grid side and the signal error of a proportional–integral (PI) outer voltage regulator is designed to reflect the change in power caused by the irradiation variation. Hence, with this information, the proposed algorithm can greatly reduce the power losses caused by the dynamic tracking errors under rapid weather changing conditions.

The superiority of the newly proposed method is supported by simulation results. Finally, the stability of the system with the proposed control scheme is investigated by considering the environmental changes. The rest of the paper is organized as follows. The mathematical model of a three-phase grid-connected PV system is shown in Section II. The current and voltage controllers for a three-phase grid-connected photovoltaic system are shown in Section III and relation of MPPT with the proposed control scheme is shown in Section IV. Section V shows the simulation results with the proposed controller under different circumstances. Finally, the paper is concluded in Section VII.

II. MODELING AND SYSTEM DESCRIPTION

Fig. 1 shows the basic structure of a single-stage three-phase grid-connected PV system studied in this paper. This system consists of a PV array, an input filter capacitor *C*, a three-phase VSI, an output filter inductor *L*, and grid. The PV modules are connected in a series–parallel configuration to match the required dc voltage and power rating. The input capacitor supports the solar array voltage for the VSI. The three-phase pulse width-modulated inverter with a filter inductor converts a dc input voltage into an ac sinusoidal voltage by means of appropriate switch signals to make the output current in phase with the utility voltage and obtain a unity power factor.

A. PV Array and Solar Cell Model

A PV generator is a combination of solar cells, connections, protective parts, supports, etc. In the present modeling, the focus is only on cells. Solar cells consist of a p-n junction; various modeling of solar cells have been proposed in the literature. Thus, the simplest equivalent circuit of a solar cell is a current source in parallel with a diode. The output of the current source is directly proportional to the light falling on the cell (photocurrent). During darkness, the solar cell is not an active device; it works as a diode, i.e., a p-n junction. It produces neither a current nor a voltage. Thus, the diode determines the *I–V* characteristics of the cell. For this paper, the electrical equivalent circuit of a solar cell is shown in Fig. 2. The output current *I* and the output voltage of a solar cell are given by

$$I = I_{Ph} - I_{d0} - \frac{V_{do}}{R_{sh}}$$
$$= I_{Ph} - I_0\left(exp\left(\frac{q.V_{do}}{n.k.T}\right) - 1\right) - \frac{V_{do}}{R_{sh}} \quad (1)$$
$$V = V_{do} - R_s I \quad (2)$$

Here, I_{ph} is the photocurrent, *I*0 is the reverse saturation current, *Id*0 is the average current through the diode, *n* is the diode factor, *q* is the electron charge (*q* = 1.6∗10−19), *k* is the Boltzmann's constant (k = 1.38∗10−23), and T is the solar array panel temperature. Rs is the intrinsic series resistance of the solar cell; this value is normally very small. R_{sh} is the equivalent shunt resistance of the solar array, and its value is very large.

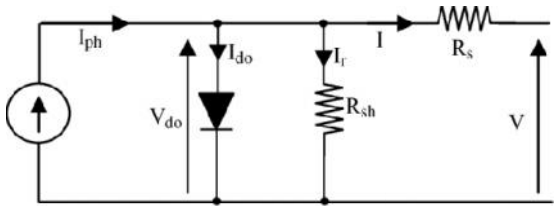

Figure 2: Electrical equivalent circuit of Solar cell.

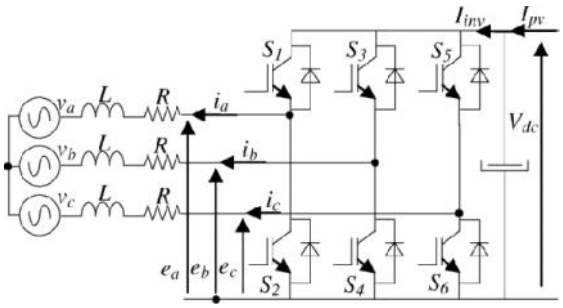

Figure 3: Three-phase VSI.

In general, the output current of a solar cell is expressed by

$$I = I_{Ph} - I_0\left(exp\left(\frac{q}{n.k.T}(V + R_s I)\right) - 1\right) - \left(\frac{V + R_s I}{R_{sh}}\right) \quad (3)$$

In (3), the resistances can be generally neglected, and thus, it can be simplified to

$$I = I_{Ph} - I_0\left(exp\left(\frac{q}{n.k.T}.V\right) - 1\right) \quad (4)$$

If the circuit is opened, the output current *I* = 0, and the open-circuit voltage *V*oc is expressed by

$$V_{oc} = \left(\frac{n.k.T}{q}\right) In\left(\frac{I_{Ph}}{I_o} + 1\right) \approx \left(\frac{n.k.T}{q}\right) In\left(\frac{I_{Ph}}{I_0}\right) \quad (5)$$

If the circuit is shorted, the output voltage *V* = 0, the average current through the diode is generally neglected, and the short circuit current *I*sc is expressed by using

$$I_{sc} = I = \frac{I_{Ph}}{\left(1 + \frac{R_S}{R_{sh}}\right)} \quad (6)$$

Finally, the output power *P* is expressed by

$$P = VI = \left(I_{ph} - I_{do} - \frac{V_{do}}{R_{sh}}\right)V \quad (7)$$

B. VOLTAGE SOURCE INVERTER (VSI) Model

The VSI connected to the grid through an *L* filter is shown in Fig. 3. In this section, a dynamic analytical model of the VSI is developed in its original three-phase *abc* frame. Then, this model is transformed into a synchronous reference frame. Before analyzing the three-phase VSI, some assumptions are proposed.

1) The three-phase voltages are sinusoidal and symmetrical, and their representations are depicted in (8).
2) The switches operate at constant frequency. The switching frequency is much higher than the line frequency.
3) The inductors *L* are linear and balanced. Saturation is not a concern.
4) The whole conduction losses are represented by three symmetrical resistors *R*, as shown in Fig. 3.
5) The absence of the zero sequence in the currents into a three wire system.

$$\begin{cases} v_a = V_m \cos(\omega t) \\ v_b = V_m \cos\left(\omega t - \frac{2}{3}\pi\right) \\ v_c = V_m \cos\left(\omega t + \frac{2}{3}\pi\right) \end{cases} \quad (8)$$

Based on the aforementioned assumptions, the model of the VSI in the stationary *abc* frame is established as

$$\begin{cases} e_a = L\frac{di_a}{dt} + i_a R + v_a + v_{nN} \\ e_b = L\frac{di_b}{dt} + i_b R + v_b + v_{nN} \\ e_c = L\frac{di_c}{dt} + i_c R + v_c + v_{nN} \\ I_{pv} = C\frac{dV_{dc}}{dt} + I_{inv} \end{cases} \quad (9)$$

By doing the sum of the three equations in (9), one can obtain the relation

$$v_{nN} = \frac{1}{3}(e_a + e_b + e_c) \quad (10)$$

The switching function *d*∗*k* (*k* = 1, 3, 5) of the inverter is defined as in

$$d_k^* = \begin{cases} 1, & if\ S_k\ is\ on\ and\ S_{k+1}\ is\ off \\ 0, & if\ S_k\ is\ off\ and\ S_{k+1}\ is\ on \end{cases} \quad (11)$$

Hence, one can write the complete model (12) of the VSI in the *abc* frame

$$\begin{cases} L\frac{di_a}{dt} = -v_a - i_a R + \left(d_1^* - \frac{d_1^*+d_2^*+d_3^*}{3}\right)V_{dc} \\ L\frac{di_b}{dt} = -v_b - i_b R + \left(d_2^* - \frac{d_1^*+d_2^*+d_3^*}{3}\right)V_{dc} \\ L\frac{di_c}{dt} = -v_c - i_c R + \left(d_3^* - \frac{d_1^*+d_2^*+d_3^*}{3}\right)V_{dc} \\ C\frac{dV_{dc}}{dt} = I_{pv} - (d_1^* i_a + d_2^* i_b + d_3^* i_c) \end{cases} \quad (12)$$

For pulse width modulation (PWM) inputs, the aforementioned model can be separated into low- and high-frequency components using the Fourier analysis. The high-frequency model is concerned with the switching behavior of the inverter and is almost neglected. The low-frequency model, which has the same expression as (12), with the switching functions $d*$ being replaced by continuous duty ratios $dk(k = 1, 3, 5) \in [0, 1]$, is much more considered

$$T_{dq0}^{abc} = \frac{2}{3}\begin{bmatrix} \cos(\omega t) & \cos\left(\omega t - \frac{2}{3}\pi\right) & \cos\left(\omega t + \frac{2}{3}\pi\right) \\ \sin(\omega t) & \sin\left(\omega t - \frac{2}{3}\pi\right) & \sin\left(\omega t + \frac{2}{3}\pi\right) \\ \frac{1}{2} & \frac{1}{2} & \frac{1}{2} \end{bmatrix} \quad (13)$$

It is noted that the model (12) is time varying and nonlinear. In order to facilitate the control, the model can be transformed into a synchronous orthogonal frame rotating at the angular frequency of the utility ω. With this time-varying transformation, given by (13), the positive sequence components at the fundamental frequency become constant.

Finally, the whole dynamic model (14) in the *dq* frame is obtained from (12) and (13)

$$\begin{bmatrix} \frac{di_d}{dt} \\ \frac{di_q}{dt} \\ \frac{dV_{dc}}{dt} \end{bmatrix} = \begin{bmatrix} -\frac{R}{L} & \omega & \frac{d_d}{L} \\ -\omega & -\frac{R}{L} & \frac{d_q}{L} \\ -\frac{d_d}{C} & -\frac{d_q}{C} & 0 \end{bmatrix} \begin{bmatrix} i_d \\ i_q \\ V_{dc} \end{bmatrix} + \begin{bmatrix} -\frac{1}{L} & 0 & 0 \\ 0 & -\frac{1}{L} & 0 \\ 0 & 0 & \frac{1}{C} \end{bmatrix} \begin{bmatrix} v_D \\ v_q \\ I_{pv} \end{bmatrix} \quad (14)$$

where

id, *iq* *d*- and *q*-axis grid currents, respectively;
vd, *vq* *d*- and *q*-axis grid voltages, respectively;
dd, *dq* *d*- and *q*-axis duty ratios.

III. CURRENT AND VOLTAGE CONTROLLERS

VOC strategy guarantees fast transient response and high static performance via internal current control loops.

A. Current Control

It can be seen from (14) that there is cross-coupling between the *d* and *q* components. However, cross-coupling can affect the dynamic performance of the regulator. Therefore, it is very important to decouple the two axes for better performance. This effect can be accomplished with the feed forward decoupling control method. Assuming that

$$v_{rd} = -V_d + d_d V_{dc} + \omega L i_q$$

$$v_{rq} = -V_q + d_q V_{dc} + \omega L i_d \quad (15)$$

where ω is the angular frequency of the utility. Then, the system model is transformed to

$$\begin{cases} \frac{di_d}{dt} = -\frac{R}{L} i_d + \frac{1}{L} v_{rd} \\ \frac{di_d}{dt} = -\frac{R}{L} i_q + \frac{1}{L} v_{rq} \\ \frac{dV_{dc}}{dt} = \frac{I_{pv}}{C} - \frac{V_d + v_{rd}}{CV_{dc}} i_d - \frac{V_q + v_{rq}}{CV_{dc}} i_q \end{cases} \quad (16)$$

The cross-coupling variables are eliminated in the aforementioned model. Hence, the currents *id* and *iq* can be controlled independently by acting upon inputs *Vd* and *Vq*, respectively. Furthermore, by using PI-type regulators, a fast dynamic response and zero steady-state errors can be achieved. The diagram of the current regulator is shown in Fig. 4. Since the switching frequency is much higher than the line frequency, the sampling and hold delay is neglected.

In the diagram, *kip* and *kii* are the proportional and integral parameters, respectively; $i*$ is the reference current signal, and *I* is the feedback current. The diagram is suitable for both *id* and *iq* loops. From the diagram, the closed-loop transfer function of the *d*, *q* current loops is

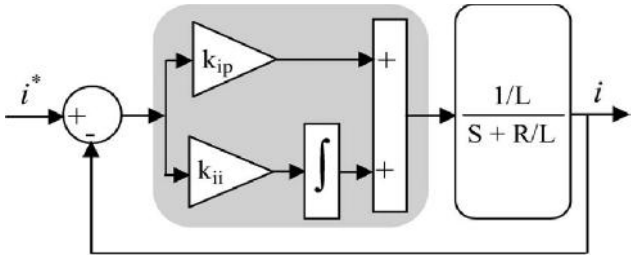

Fig. 4. Current loop diagram.

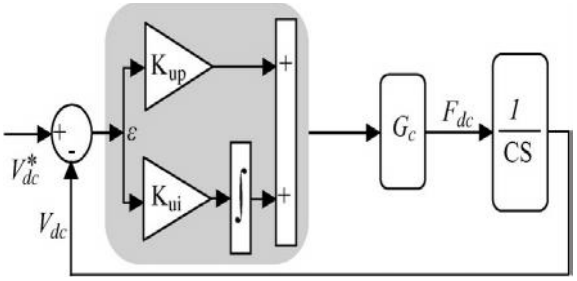

Fig. 5. Voltage loop diagram with constant irradiation.

$$\frac{i_q(s)}{i_q^*(s)} = \frac{i_d(s)}{i_d^*(s)} = \frac{K_{ip}}{L}\frac{S+\frac{k_{ii}}{k_{ip}}}{S^2+\frac{k_{ip}+R}{L}+\frac{k_{ii}}{L}} \quad (17)$$

The damping ratio $\zeta = (k_{ip} + R)/2L\sqrt{(k_{ii}/L)}$, and $\omega^2_{ni} = k_{ii}/L$. Thus, the parameters of the current regulator can be designed as follows:

$$k_{ip} = 2\zeta\omega_{ni}L - R$$

$$k_{ii} = L\omega_{ni}^2 \quad (18)$$

Voltage Control

In the case of a unity power factor (iq = 0) and with the previous assumption, the third equation in the model (14) is repeated as

$$C\frac{dV_{dc}}{dt} = I_{pv} - d_d i_d. \quad (19)$$

At the beginning of a sequence, the atmospheric conditions are considered constant; hence, an equivalent input is defined as

$$F_{dc} = I_{pv} - d_d i_d \quad (20)$$

In order to regulate the dc voltage at a fixed value, the error $\varepsilon = V*\mathrm{dc} - V\mathrm{dc}$ is passed through a PI-type compensator, as shown in Fig. 5.

In the diagram, the voltage loop is an outer loop, while the current loop is an inner loop. The internal loop has been designed to achieve short settling times in order to achieve a fast correction of the error. The outer loop can be designed to be slower.

Thus, the inner and outer loops can be considered decoupled, and they can be linearized. Consequently, the current loop transfer function is approximately considered as Gc=1.

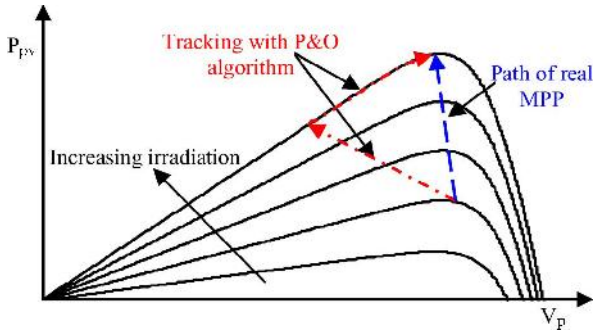

Fig. 6. Deviation from the MPP with the P&O algorithm under rapidly changing irradiance.

The closed-loop transfer function of dc voltage regulation, obtained from Fig. 3, has the following form:

$$\frac{V_{dc}(s)}{V_{dc}^*(s)} = \frac{k_{up}}{c}\frac{\frac{k_{ui}}{k_{up}}+S}{S^2+\frac{k_{up}}{c}S+\frac{k_{ui}}{c}} \quad (21)$$

In the same way as the design process of the current loop, the voltage regulator parameters can be given as follows:

$$K_{up=2\zeta C\omega_{nu}}$$

$$K_{ui} = C\omega_{nu}^2. \quad (22)$$

IV MPPT ALGORITHM

MPPT technique adjust the PV array voltage in order to extract available maximum power under any atmospheric changes. Maximum Power Point Tracking, frequently referred to as MPPT, is an electronic system that operates the Photovoltaic (PV) modules in a manner that allows the modules to produce all the power they are capable of. MPPT is not a mechanical tracking system that "physically moves" the modules to make them point more directly at the sun. MPPT is a fully electronic system that varies the electrical operating point of the modules so that the modules are able to deliver maximum available power. Additional power harvested from the modules is then made available as increased battery charge current. MPPT can be used in conjunction with a mechanical tracking system, but the two systems are completely different.

The dc voltage controller is used to produce the reference current value for the *id* current controller. Its aim is to keep the voltage constant on the dc side in normal condition or during rapidly changing atmospheric conditions. The MPPT algorithm modulates the reference voltage $V*\mathrm{dc}$ according to the environmental conditions in order to keep the operating point of the PV panels close to the MPP. In

the conventional P&O method, the MPP is obtained from the PV array power by multiplying the voltage and current of PV arrays and comparing it with the previously measured power. In the case of a sudden increase in irradiance, the P&O algorithm reacts as if the increase occurred as a result of the previous perturbation of the array operating voltage. The next perturbation, therefore, will be in the same direction as the previous one. Assuming that the system has been initially oscillating around the MPPT, the path of this behavior is drawn in Fig. 6. It can be seen that a continuous perturbation in one direction will lead to an operating point far away from the actual MPP. This process continues until the increase in irradiance slows down or ends.

In order to overcome the limitations of the P&O method, the proposed MPPT enables us to decouple the change in power caused by the simultaneous increment perturbation and irradiation variation. The irradiation variation is estimated by using the signal error of the PI controller of the dc voltage control. The PI regulator is designed to assure zero signal error if the atmospheric conditions are constant and a constant signal error in the opposite case. Hence, the signal error reflects only the change in power caused by the irradiation variation. After that, in order to calculate the total change in the PV array power, the *d*-axis grid current component is used. Finally, the change in power caused by the previous perturbation is obtained by a simple subtraction; therefore, the correct direction of the MPP can be identified.

A. *Procedure for PV Power Calculation*

In the synchronous rotating frame *d*, *q*, the active and reactive powers of a three-phase grid-connected VSI are given by

$$\begin{cases} P = \frac{3}{2}(V_d i_d + V_q i_q) \\ Q = \frac{3}{2}(V_d i_d - V_q i_q) \end{cases} \quad (23)$$

If the three-phase grid voltage is ideally sinusoidal without any harmonics, then in the *d*, *q* frame, the grid voltage vector is given by

$$\begin{cases} V_d = V \\ V_q = 0 \end{cases} \quad (24)$$

In practice, the grid voltage is non sinusoidal due to harmonics. Therefore, both *Vd* and *Vq* will not be constant but have slight ripples whose frequencies and magnitudes depend on the harmonic components. However, in steady state, the average value of *Vq* is still equal to zero. Consequently, (23) can be rewritten as (25). Its active power depends on the *d*-axis current, and the reactive power depends on the *q*-axis current. Furthermore, in order to achieve unity power factor fundamental current flow, the *q* component of the command current vector is set to zero

$$\begin{cases} P = \frac{3}{2}(V_d i_d) \\ Q = \frac{3}{2}(V_d i_q) \end{cases} \quad (25)$$

Assuming ideal power transmission between solar array and grid line, the relationship of instantaneous active power exchanged between the PV array and the grid is given by

$$P_v = P = \frac{3}{2}(v_d i_d) \quad (26)$$

This allows one to obtain the relation

$$i_d = \frac{2}{3v_d} P_{pv} \quad (27)$$

Therefore, the PV power information can be obtained from the *d*-axis grid current component by the relation (27).

B. *Outer Voltage Regulator Signal Error*

The change of d-axis current in one period sampling Te under irradiation variation is expressed by the following:

$$\Delta i_d(k) = \Delta i_v(k) + \Delta i_G(k) \quad (28)$$

Δ*iv*(*k*) is the change of *d*-axis current component caused by the tracker perturbation, and Δ*iG*(*k*) is the change of *d*-axis current component caused by the change in irradiation Fig. 7. Thus, the dc bus-voltage control loop under changing irradiation can be modeled with the block diagram of Fig. 8, where the current of PV array is an input disturbance. In this case, the error

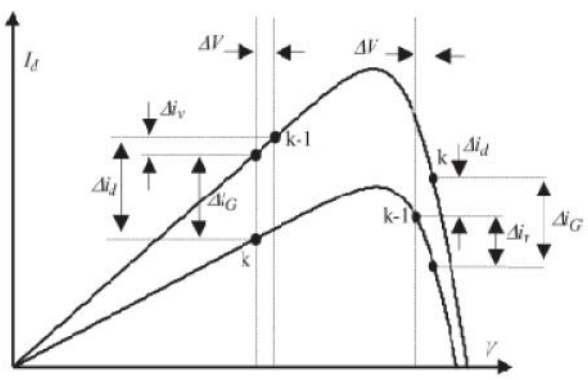

Fig. 7. I_d–V characteristic under variable irradiation

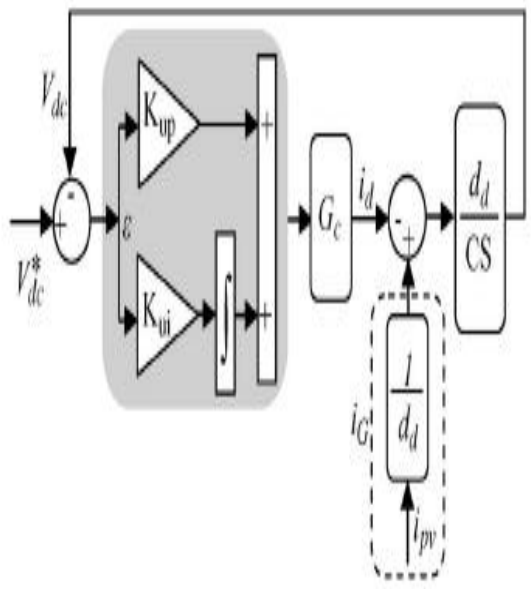

Fig. 8. Equivalent diagram of Voltage loop under variable irradiation.

between voltage reference $V*$ dc and voltage measurement Vdc is the following:

$$\varepsilon(s) = A(s)V^*_{dc}(s) + B(s)i_G(s) \quad (29)$$

where

$$A(s) = \frac{CS^2}{CS^2 + d_d k_{up} S + d_d k_{ui}}$$

$$B(s) = \frac{d_d}{C} \frac{S}{S^2 + \frac{d_d k_{up}}{C} S + \frac{d_d k_{ui}}{C}}$$

If we consider only the impact of perturbation iG, we can write

$$\varepsilon(s) = \frac{d_d}{C} \frac{S}{S^2 + \frac{d_d k_{up}}{C} S + \frac{d_d k_{ui}}{C}} i_G(s) \quad (30)$$

Assuming that the rate of change in the irradiation is constant over one sampling period Te of the MPPT ($\Delta iG = \alpha.T\,e$), the $iG(s)$ expression can be written

$$i_G(s) = \frac{\alpha}{S^r} \quad (31)$$

By inserting (31) into (30), the error is defined as

$$\varepsilon(s) = \frac{d_d}{C} \frac{\alpha}{S^3 + \frac{d_d k_{up}}{C} S^2 + \frac{d_d k_{ui}}{C} S} \quad (32)$$

To calculate the signal error, we use the final value theorem for Laplace transforms. According to this theorem, as long as $\varepsilon(s)$ does not have any poles in the right half of the complex plane, except maybe $s = 0$, then

$$\varepsilon = \lim_{s \to 0} \left[\frac{d_d}{C} \frac{\alpha}{S^2 + \frac{d_d k_{up}}{C} S + \frac{d_d k_{ui}}{C}} \right] \quad (33)$$

Hence, the signal error has the following form (Fig. 9):

$$\varepsilon = \frac{\alpha}{k_{ui}} \quad (34)$$

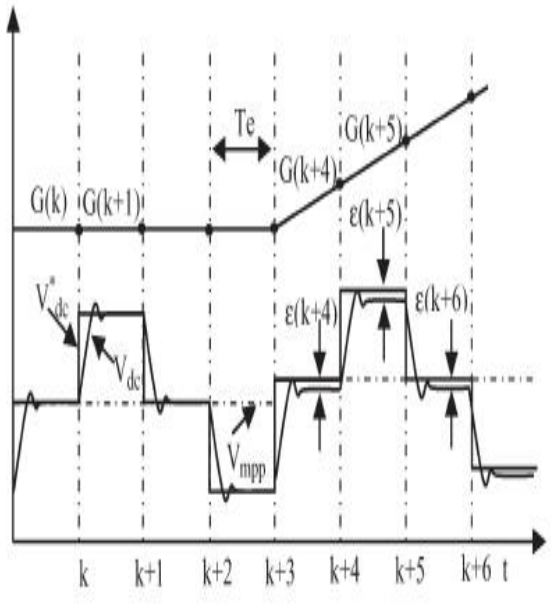

Fig. 9. Voltage waveform under variable irradiation.

ISSN 2321-6905

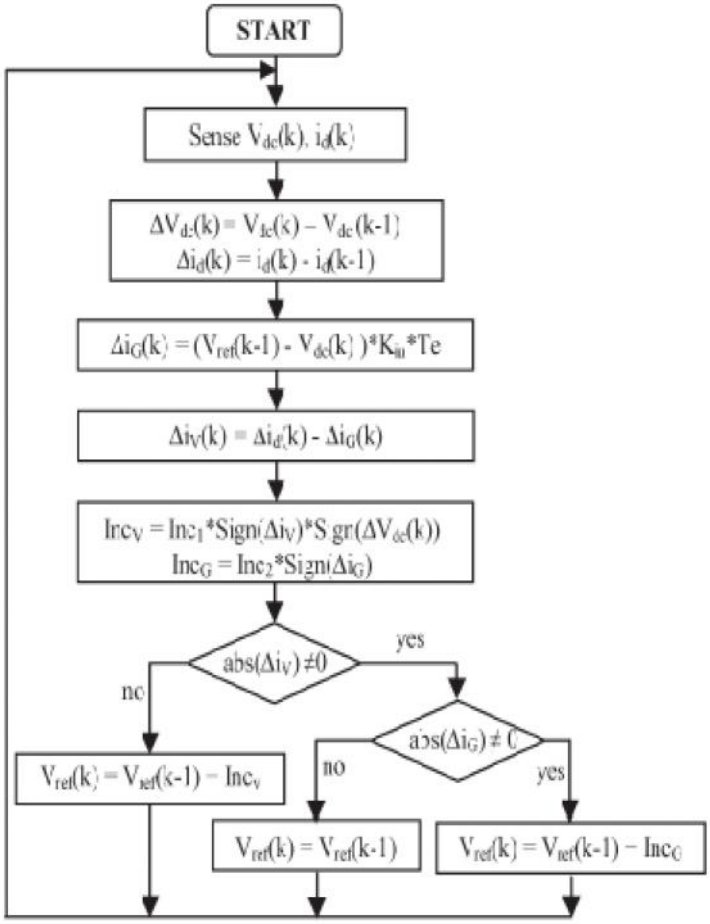

Fig. 10. Flowchart of the proposed MPPT algorithm behavior.

Finally, the Δ*iG*(*k*) that reflects only the change in power caused by the irradiation variation is defined as in

$$\Delta i_G = T_e \varepsilon k_{ui} = T_e k_{ui}.\left(V_{dc}^{*}(k-1) - V_{dc}(k)\right) \qquad (35)$$

The flowchart of the proposed MPPT is shown in Fig. 10. The first step is to set up a fixed voltage whose value is about 0.8 times of the PV array open-circuit voltage. Then, the instantaneous voltage of the PV array and the *d*-axis grid current component are measured using the saved previous voltage and current in order to calculate the differential values of Δ*id* and Δ*V*dc. After that, the Δ*iG* and Δ*iV* are calculated by using (35) and (28), respectively. With this information, two increments are calculated. The first *IncV* will be used when the PV array voltage is far away from the MPP voltage and the second *IncG* when irradiance change is present and the PV array voltage is initially equal to the voltage of the MPP. In the next test, if abs(Δ*iV*) is more than zero (the power change caused by the previous tracker perturbation is different from zero), the reference voltage of the PV array is given by adding *IncV* to the previous reference voltage (*IncV* can be positive or negative, depending on the sign of Δ*V*dc and Δ*iV*). In the opposite case, the reference voltage is incremented with *IncG* (*IncG* can be positive or negative in function of the sign of Δ*iG*) if abs(Δ*iG*) is more than zero (irradiance change is present), when Δ*iG* is equal to zero; the reference voltage increment is set to zero.

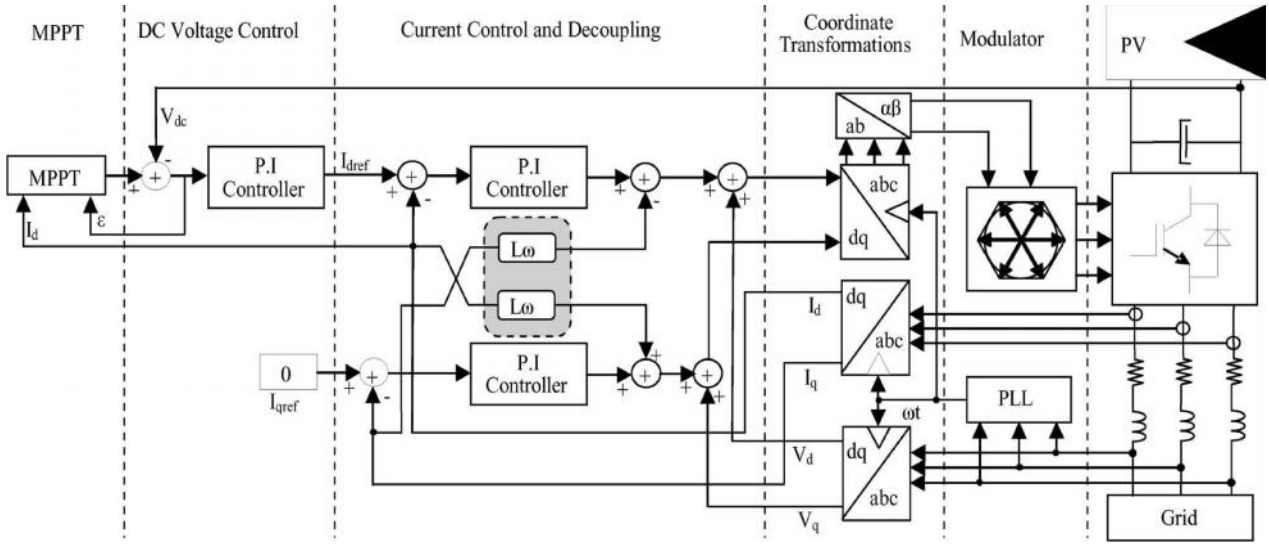

Fig. 11.Block diagram of Grid-connected PV system with the proposed MPPT algorithm.

V. SIMULATION RESULTS

This section presents the simulation results of the conventional P&O and the proposed method in order to validate the performance of the control scheme. Computer simulation has been done using MATLAB/SIMULINK simulation package (Version 7.8.0 R2009a). The full diagram of the control methodology and the modulation is shown in Fig. 11. The PV module provides 60 W of nominal maximum power and a 21.1-V open-circuit voltage at an irradiation of 1 kW/m2 and an ambient temperature of 25 ◦C. To compare the performance of the proposed MPPT method with that of the P&O method, the simulations are configured under exactly the same conditions to compare the performances.

The PV array in simulation is composed of ten series connected modules. The sampling period used for MPPT algorithm is chosen as 0.2 s, and voltage increments of *Inc1* = 0.5 V and *Inc2* = 0.1 V are used.

In order to verify the effect of rapidly changing irradiation, an irradiation ramp change was used. A 20-s period for the increasing and decreasing ramps was selected. This irradiation change starts from 200 W/m2, stops at 1000 W/m2, waits at this level for 20 s, and decreases again back to 200 W/m2 with a constant slope. The temperature is considered constant during the simulation.

Figs. 12 and 13 show the simulation results of the steady state and dynamic responses of the classical P&O method. The results verified that the MPPT method has very poor performance under dynamic response.

In Fig. 12 and under a decrease of irradiation (50–70 s), we can see that the voltage of PV array varies between V and V +Δv since it decreases the PV array power in the two directions of perturbation. This is because the power change caused by irradiation decrease in sunshine is greater than the variation caused by the voltage perturbation.

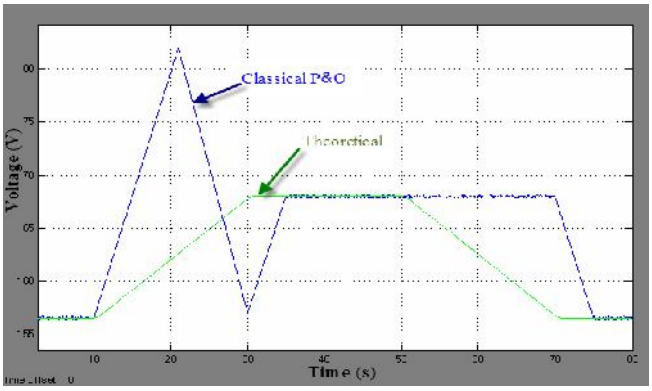

Fig. 12. PV array voltage with classical P&O and theoretical MPP voltage during a trapezoidal irradiation profile.

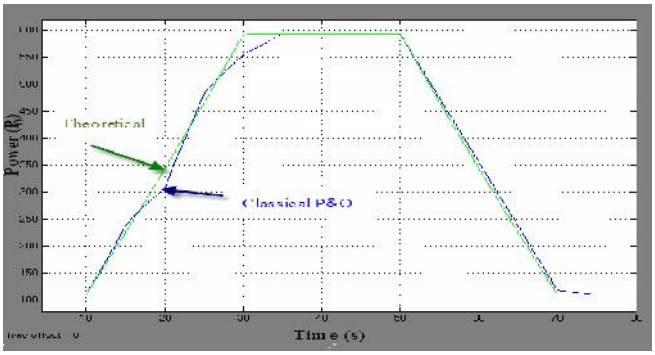

Fig. 13. Simulation measurement of the PV array power during a trapezoidal irradiation profile, using the classical P&O MPPT method, compared to the theoretical MPP power.

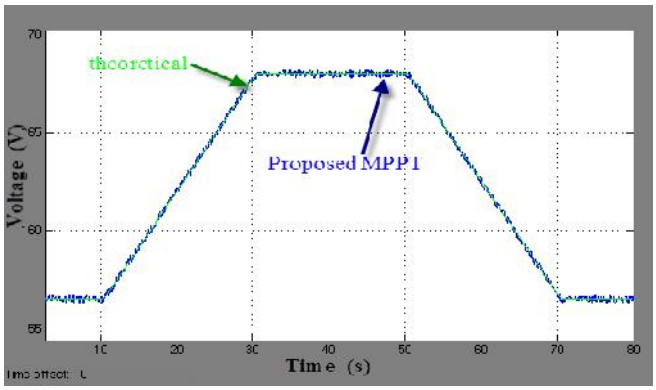

Fig. 14. PV system voltage with the proposed MPPT and theoretical MPP voltage during a trapezoidal irradiation profile.

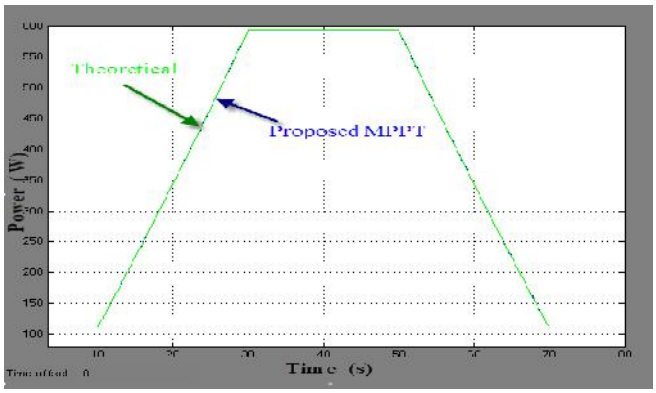

Fig. 15. Simulation measurement of the PV array power during a trapezoidal irradiation profile, using the proposed MPPT method, compared to the theoretical MPP power.

Fig. 14 shows the terminal voltage of the PV array compared with the theoretical MPP voltage. Fig. 15 shows the theoretical power and the maximum power obtained from the proposed MPPT. From this figure, we can see the control system efficiently tracks the maximum power at any conditions.

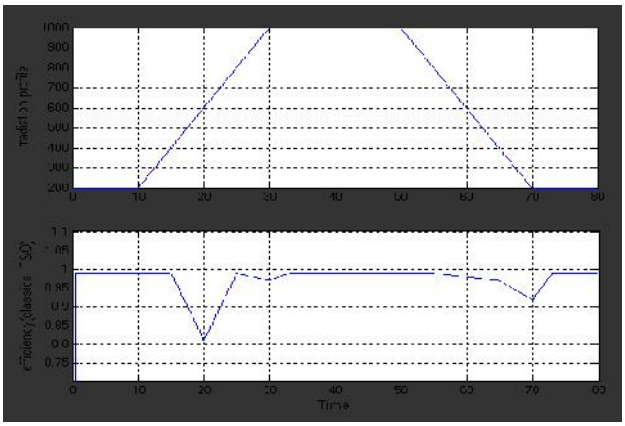

Fig. 16. Simulation measurement of the instantaneous efficiency with classical P&O during a trapezoidal irradiation profile.

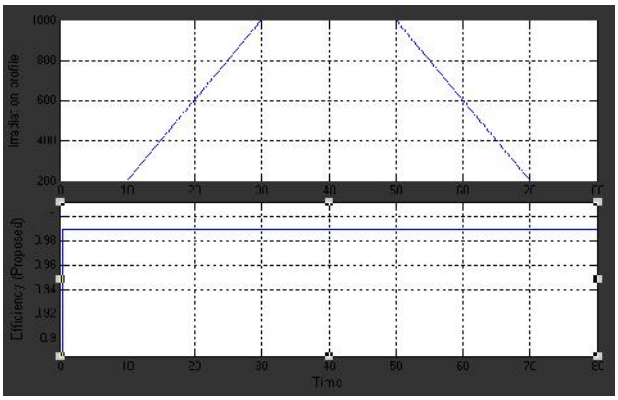

Fig. 17. Simulation measurement of the instantaneous efficiency with proposed MPPT during a trapezoidal irradiation profile.

From the simulation Figs. 16 and 17, during the irradiation change, the classical P&O method has a poor instantaneous efficiency, while the proposed method tracks the MPPT with the same efficiency as in the steady-state operation.

From the results it is clear that the designed controller performs well at varying atmospheric conditions and provides robust performance. The corresponding control signals are shown in above figures.

VII. CONCLUSION

The control problem of grid-connected photovoltaic arrays is stated as to provide the maximum of power irrespective of the solar irradiance conditions. The main objective of this paper is, to avoid possible mistakes of the classical P&O algorithm due to the fast-changing irradiation. This paper has proposed an improved MPPT controller without PV array power measurement. This MPPT method permits one to differentiate the contribution of increment perturbation and irradiation change in power variation, hence identifying the correct direction of the MPP. The steady-state and dynamic responses illustrated the perfect desired reference tracking controller. Moreover, the output power losses caused by the dynamic tracking errors are significantly reduced, particularly under fast changing irradiation. The proposed control algorithm is simple, robust and easy to implement in real time applications. The MATLAB®/Simulink® numerical simulations have shown that the proposed scheme is quite effective at tracking strongly variable irradiance conditions.

REFERENCES

[1] C. Meza, J. J. Negroni, D. Biel, and F. Guinjoan, "Energy-balance modeling and discrete control for single-phase grid-connected PV central inverters," *IEEE Trans. Ind. Electron.*, vol. 55, no. 7, pp. 2734–2743, Jul. 2008.

[2] B. Sahan, A. N. Vergara, N. Henze, A. Engler, and P. Zacharias, "A singlestage PV module integrated converter based on a low-power currentsource inverter," *IEEE Trans. Ind. Electron.*, vol. 55, no. 7, pp. 2602–2609, Jul. 2008.
[3] K. Hemmes, "Towards multi-source multi-product and other integrated energy systems," *Int. J. Integr. Energy Syst.*, vol. 1, no. 1, pp. 1–15, Jan.–Jun. 2009.
[4] F. Liu, Y. Zhou, S. Duan, J. Yin, B. Liu, and F. Liu, "Parameter design of a two-current-loop controller used in a grid-connected inverter system with *LCL* filter," *IEEE Trans. Ind. Electron.*, vol. 56, no. 11, pp. 4483–4491, Nov. 2009.
[5] T. Shimizu, O. Hashimoto, and G. Kimura, "A novel high-performance utility-interactive photovoltaic inverter system," *IEEE Trans. Power Electron.*, vol. 18, no. 2, pp. 704–711, Mar. 2003.
[6] T. Esram, J. W. Kimball, P. T. Krein, P. L. Chapman, and P. Midya, "Dynamic maximum power point tracking of photovoltaic arrays using ripple correlation control," *IEEE Trans. Power Electron.*, vol. 21, no. 5, pp. 1282–1291, Sep. 2006.
[7] N. Femia, G. Petrone, G. Spagnuolo, andM. Vitelli, "Optimization of perturb and observe maximum power point tracking method," *IEEE Trans. Power Electron.*, vol. 20, no. 4, pp. 963–973, Jul. 2005.
[8] G. Carannante, C. Fraddanno, M. Pagano, and L. Piegari, "Experimental performance of MPPT algorithm for photovoltaic sources subject to inhomogeneous insolation," *IEEE Trans. Ind. Electron.*, vol. 56, no. 11, pp. 4374–4380, Nov. 2009.

HIMA BINDU S currently pursuing her M.Tech in Electrical Power Systems from TRR Engineering College, Hyderabad, Telangana, India affiliated to JNTU University, Hyderabad. She has done her B.Tech degree from Ellenki College of Engineering and Technology, affiliated to JNT University, Hyderabad, Telangana, India and her fields of interest include Renewable Energy Sources, Power Systems and Industrial Drives.

BHARGAV RAM T working as Associate Professor in TRR Engineering College, Hyderabad, Telangana, India affiliated to JNTU University, Hyderabad with 12 years of experience in teaching and various fields. His fields of interest include Non Conventional Energy Sources and Power Systems.